Hindawi
Shock and Vibration
Volume 2019, Article ID 7585401, 17 pages
https://doi.org/10.1155/2019/7585401

Research Article

Roller Bearing Fault Diagnosis Based on Adaptive Sparsest Narrow-Band Decomposition and MMC-FCH

Yanfeng Peng,[1,2] Junhang Chen,[1,2] Yanfei Liu,[1,3,4,5] Junsheng Cheng,[4,5] Yu Yang,[4,5] He Kuanfang,[6] Guangbin Wang,[1,2] and Yi Liu[7]

[1]*Hunan Provincial Key Laboratory of Health Maintenance for Mechanical Equipment, Hunan University of Science and Technology, Xiangtan 411201, China*
[2]*Engineering Research Central of Advanced Mining Equipment, Ministry of Education, Hunan University of Science and Technology, Xiangtan 411201, China*
[3]*School of Mechanical Engineering, Hunan University of Science and Technology, Xiangtan 411201, China*
[4]*State Key Laboratory of Advanced Design and Manufacturing for Vehicle Body, Hunan University, Changsha 410082, China*
[5]*College of Mechanical and Vehicle Engineering, Hunan University, Changsha 410082, China*
[6]*Department of Mechatronics, Foshan University, Foshan, Guangdong 528000, China*
[7]*Zhuzhou National Innovation Railway Technology Co., Ltd, Zhuzhou 412000, China*

Correspondence should be addressed to Yanfei Liu; 783713797@qq.com

Received 24 February 2019; Accepted 27 June 2019; Published 29 July 2019

Academic Editor: Franck Poisson

Adaptive sparsest narrow-band decomposition (ASNBD) method is proposed based on matching pursuit (MP) and empirical mode decomposition (EMD). ASNBD obtains the local narrow-band (LNB) components during the optimization process. Firstly, an optimal filter is designed. The parameter vector in the filter is obtained during optimization. The optimized objective function is a regulated singular local linear operator so that each obtained component is limited to be a LNB signal. Afterward, a component is generated by filtering the original signal with the optimized filter. Compared with MP, ASNBD is superior in both the physical meaning and the adaptivity. Drawbacks in EMD such as end effect and mode mixing are reduced in the proposed method because the application of interpolation function is not required. To achieve the fault diagnosis of roller bearings, raw signals are decomposed by ASNBD at first. Then, appropriate features of the decomposed results are chosen by applying distance evaluation technique (DET). Afterward, different faults are recognized by utilizing maximum margin classification based on flexible convex hulls (MMC-FCH). Comparisons between EMD and ASNBD show that the proposed method performs better in the antinoise performance, accuracy, orthogonality, and extracting the fault features of roller bearings.

1. Introduction

Analysis methods for vibration signals play an important role in mechanical fault diagnosis. Techniques like matching pursuit (MP) [1–3] and empirical mode decomposition (EMD) [4, 5] have been widely used for analyzing vibration signals of mechanical components recently.

EMD method, which was proposed by Huang [4], is a suitable method for nonstationary signal analysis. As the extremas of an original signal is calculated, the signal is divided into several intrinsic mode functions (IMFs) with physical meaning when EMD is applied. EMD has been proved to be effective in the fields such as fault diagnosis [6], condition monitoring [7], and image identification [8]. Nevertheless, some disadvantages including mode mixture [9, 10] and end effect [11, 12] are existed in EMD as interpolation function is involved in the calculation process.

MP was brought forward by Mallat [1] in 1993. Various dictionaries are utilized to gain the sparsest decomposition results of an original signal. MP has been used in many areas since it was proposed [13–17]. Nevertheless, the highly redundant dictionary must be selected beforehand, and the

physical meaning of the obtained decomposition results are not explicit enough when MP is used; thus, the application range of MP is limited [3].

An adaptive time-frequency approach for nonstationary signal analysis, namely, adaptive sparsest narrow-band decomposition (ASNBD) is proposed based on the basic idea of MP and EMD [18]. ASNBD decomposes an original signal into several local narrow-band (LNB) signals [19]. An optimal filter must be determined at first in ASNBD method. The filter parameters are defined during the optimization process. The optimized objective function is a regulated operator [19] so that each obtained component is limited to be a LNB signal. Afterward, a component is generated by utilizing the optimized filter. The obtained components are constrained to be LNB signals as a regulated differential operator is applied as the objective function.

The similarity between ASNBD and EMD is that both the two methods can generate a series of meaningful component. However, to gain the decomposition results, an optimization method is applied in ASNBD instead of calculating the envelopes of the extreme points in EMD. Compared to other improved EMD methods, as the calculation of extreme points is inevitable [10], the accompanied disadvantages such as mode mixing and end effect are alleviated.

An optimization problem has to be solved to gain the sparsest representation in both MP and ASNBD. Nevertheless, the construction of a highly redundant dictionary is no more needed in ASNBD before the method is applied. Meanwhile, the generated components are LNB signals with physical meaning. Therefore, compared to MP, ASNBD is better at either the adaptivity or the physical meaning. In short, ASNBD is inspired by the basic theory of EMD and MP and proposed by avoiding their disadvantages and learning their advantages.

The maximum margin classification based on flexible convex hulls (MMC-FCH), which was inspired by SVM, was proposed by Zeng [20, 21]. The class regions of the sample sets are approximated by convex hulls of the training samples in SVM. The convex hull of SVM is an unrealistic approximation of the class region of the samples when the samples are not enough. MMC-FCH was proposed aiming at solving the problems accompanied with the application of convex hull by extending the flexible convex hulls. As MMC-FCH was used to recognize rolling element faults and showed a satisfactory performance in reference [20], it is chosen to fulfill the fault diagnosis in the paper.

Firstly, the raw signals are decomposed by using ASNBD and the features of the components are generated. Then, the dimensions of the features are reduced by distance evaluation technique (DET) [22, 23] to improve classification accuracy. Finally, MMC-FCH is applied for classifying the fault type of the bearing.

The paper is organized as follows. ASNBD is proposed in section 2. In section 3, descriptions about feature selection are given. In section 4, the MMC-FCH algorithm is given out. In section 5, the procedure of the proposed method is stated, and the effectiveness of is verified by experimental and simulation signals. The conclusions are given in the end.

2. ASNBD

2.1. Vibration Model. Vibration impulses appear when a fault occurred on the roller bearing [24], and the collected vibration signals are modulated by the corresponding impulses. Therefore, the signal model can be described as [25]

$$x(t) = \sum_{i=-\infty}^{+\infty} h(t - iT)q(iT) + n(t), \tag{1}$$

$h(t)$ is the impulse signal, $x(t)$ is the fault signal, $D(r_{i-1}(n) - \mathrm{INBC}_i(n))$ denotes the periodic modulation, and $n(t)$ is the noise disturbance. Besides, discrete time and continuous time are denoted as "n" and "t" in this paper, respectively.

It can be inferred from Fourier transform (FT) that $h(t)$ is consist of several cosine signals. The vibration signal is a relative narrow-band signal. Hence, the model of the vibration signal $x(t)$ is as follows:

$$x(t) = s(t) + n(t), \tag{2}$$

$s(t) = \sum_{i=-\infty}^{+\infty} a_i(t) g_i(\omega t + \varphi(t))$ is the modulated signal and $a_i(t) g_i(\omega t + \varphi(t))$ is a narrow-band signal. The definition of LNB signal is stated in the following section.

2.2. Definitions of LNB and INBC. For a given signal, if any neighborhood range of the data points can be regarded as a narrow-band signal, the given signal is a local narrow-band (LNB) signal [19].

If a generated component satisfies the conditions of LNB signal, then it can be regarded as an intrinsic narrow-band component (INBC).

2.3. Singular Local Linear Operator (SLLO). For an operator T, if there is a neighborhood range B_t,

$$T(S)(t) = T\left(S|_{B_t}\right)(t), \tag{3}$$

$S|_{B_t} = S(t)$ when $t \in B(t)$, and 0; otherwise, T is a SLLO [19].

A singular local linear operator T proposed in reference [19] is used by the ASNBD method.

$$T = \left(\frac{1}{\omega^2}\frac{d^2}{dt^2} + 1\right)^2. \tag{4}$$

2.4. ASNBD Procedure. For an original signal $x(n)$, the ASNBD algorithm is as follows:

(1) Set $r_0(n) = x(n)$ and $i = 1$, $n = 1, 2, \ldots, N$.

(2) Construct the optimal problem P_1:

$$P_1: \mathrm{Minimize} \left\|T(\mathrm{INBC}_i(n))\right\|_2^2 + \lambda \left\|D(r_{i-1}(n) - \mathrm{INBC}_i(n))\right\|_2^2. \tag{5}$$

T is given in equation (4). Minimizing $\|T(\mathrm{INBC}_i(n))\|_2^2$ indicates that $\mathrm{INBC}_i(n)$ is a LNB signal. $D(r_{i-1}(n) - \mathrm{INBC}_i(n))$ is the differentiation of $r_{i-1}(n) - \mathrm{INBC}_i(n)$. $D(r_{i-1}(n) - \mathrm{INBC}_i(n))$ is applied for regulating the residue. λ is the weight parameter, which is set to 17 in the experiments of this paper. It is worth mentioning

that in the optimal problem P_2, all the data in $\mathrm{INBC}_i(n)$ is optimized, which needs a big amount of calculation.

(3) Set $r_i(n) = r_{i-1}(n) - \mathrm{INBC}_i(n)$.

(4) If $\|r_i(n)\|_2^2 < \varepsilon$, stop. If not go to step 2 and set $i = i + 1$.

To reduce the calculated amount in step (2), the optimization problem P_1 is replaced with the optimization procedure as below, and the genetic algorithm (GA) is applied to solve the optimal problem. The approach for solving the nonlinear optimization problem P_1 is as follows. Meanwhile, Figure 1 shows the calculation process of ASNBD.

(1) The FFT of $r_i(n)$ is calculated as $\hat{r}_i(k)$.

(2) The filter $\chi(k \mid \eta) \cdot (\eta = [\omega, \omega_b, \omega_c])$ is as follows (see also Figure 2):

$$\chi(k \mid \eta) = \begin{cases} \sin\omega\left[k - \omega_c + \omega_b + \pi/(2\omega)\right], & \omega_c - \omega_b - \pi/(2\omega) \le k < \omega_c - \omega_b, \\ 1, & \omega_c - \omega_b \le k \le \omega_c + \omega_b, \\ \cos\omega\left(k - \omega_c - \omega_b\right), & \omega_c + \omega_b < k \le \omega_c + \omega_b + \pi/(2\omega), \\ 0, & \text{else}. \end{cases} \tag{6}$$

(3) The optimal problem P_2 as below is solved by GA:

$$P_2: \text{Minimize} \left\|T\left[I_i(n)\right]\right\|_2^2 + \lambda\left\|D\left[r_i(n) - I_i(n)\right]\right\|_2^2. \tag{7}$$

The optimal is η_o gained during the optimization process. $I_i(n)$ equals the inverse fast Fourier transformation (IFFT) of $\chi(k \mid \eta)\hat{r}_i(k)$.

(4) Set $\mathrm{INBC}_i(n)$ to be $I_i(n)$.

2.5. Comparison between ASNBD and EMD. To verify the validity of ASNBD, a simulation signal $x_1(n)$ is analyzed:

$$\begin{aligned} x_1(n) = {} & [1 + 0.5\cos(10\pi n)]\cos[180\pi n + \sin(15\pi n)] \\ & + \cos(120\pi n)e^{-t^2}, \quad n = 0 : 1/2048 : 1, \end{aligned} \tag{8}$$

$x_1(n)$ is consist of an AM-FM signal and an attenuating signal. Figures 3(a)–3(c) are the waveforms of $x_1(n)$, the AM-FM component, and the attenuating component, respectively.

$x_1(n)$ is decomposed by EMD and ASNBD (mirror extension [26] is used to reduce end effect in this paper). Figures 4 and 5 show the analysis results. The INBCs are basically the same with the real signals, the results gained by EMD have obviously mixed modes.

To compare the decomposing results, the parameters such as the index of orthogonality IO, the correlation coefficient r_i, the rate of energy error E_i, and time T are considered, which are defined in equations (9)–(11). E_i and r_i are used to evaluate the effectiveness of ASNBD. IO and T are applied to compare the orthogonality and the computational efficiency of ASNBD and EMD, respectively.

Table 1 shows the calculated parameters. E_i of the components generated by EMD is much bigger than that obtained by ASNBD. And the INBCs are more close to the actual signals compared to EMD. Thus, the results obtained by ASNBD are more accurate than EMD. Meanwhile, the IO of ASNBD is smaller which shows the orthogonality is better. Nevertheless, ASNBD still spends more time, which is one drawback in ASNBD.

$$E_i = \frac{\sum_{n=1}^{N}\left(S_i(n) - I_i(n)\right)^2}{\sum_{n=1}^{N} I_i(n)^2}, \tag{9}$$

$$r_i = \frac{\sum_{n=1}^{N}\left(S_i(n) - \overline{S}_i\right)\left(I_i(n) - \overline{I}_i\right)}{\sqrt{\sum_{n=1}^{N}\left(S_i(n) - \overline{S}_i\right)^2 \sum_{n=1}^{N}\left(I_i(n) - \overline{I}_i\right)^2}}, \tag{10}$$

$$IO = \sum_{n=1}^{N}\sum_{n=1}^{M}\sum_{n=1}^{M} \frac{S_i(n)S_j(n)}{x^2(n)}. \tag{11}$$

For comparing the antinoise performance, $x_2(n)$ composed of an intermittent noised signal with different signal-to-noise ratios (SNRs) is applied:

$$x_2(n) = \cos\left[60\pi n + \sin\left(8\pi n^2\right)\right] + s(n), \quad n = 0 : 1/2048 : 1. \tag{12}$$

SNR is obtained as follows:

$$\mathrm{SNR} = 10\log_{10}\frac{\sum_{n=1}^{N}\left(x(n) - s(n)\right)^2}{\sum_{n=1}^{N} s(n)^2}. \tag{13}$$

Signal $x_2(n)$ (SNR equals 5, 10, or 15 dB) and the components are shown in Figure 6. The results generated by EMD and ASNBD are given in Figures 7–9. It can be seen from the figures that there exists severe mode mixing of the components obtained by EMD (labeled by the red line) because of the noise interference. ASNBD can restrain mode mixing effectively. The INBC_1 generated by ASNBD is in excellent accordance with the AM-FM component of $x_2(n)$.

In Table 2, the calculated parameters are given. The parameters indicate that ASNBD method excels EMD method both in possessing better orthogonality and the decomposition accuracy when the SNR varies.

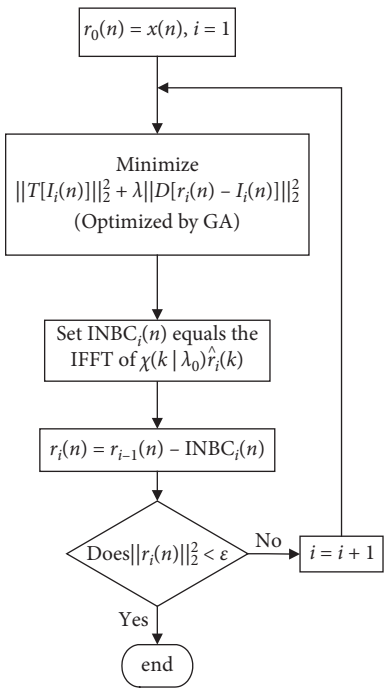

Figure 1: The flow chart of ASNBD.

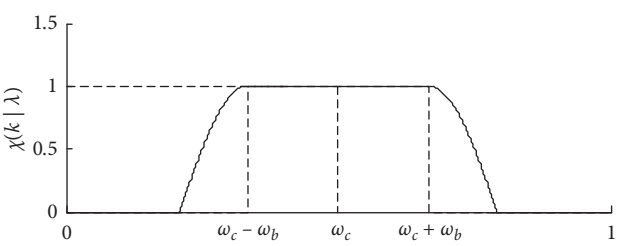

Figure 2: The filter given in equation (6).

Therefore, at least for the signals shown in Figure 6, ASNBD excels EMD both in orthogonality and accuracy, which means that ASNBD is more effective than EMD when utilized to the simulation signals with different SNRs.

The simulation analysis results indicate that ASNBD excels EMD in the accuracy, the orthogonality, and the antinoise performance when applied to the simulation signals above.

3. Feature Selection

After every raw data set is decomposed into several components, different features of the data sets can be obtained by calculating various statistical parameters. For providing enough feature information for selection, some common time and frequency domain statistical parameters shown in Table 3 are applied to extract the fault feature.

It is noted that not all features could positively affect the identification of bearing faults. Thus, useful features which are usually called as salient features have to be chosen. DET [22, 23] is applied to get salient features, and the procedure of DET is illustrated as follows:

(1) The mean distance is calculated. $p_{i,j,k}$ is the jth feature of the kth sample with the ith condition. C, J, and N_i are the number of conditions, features, and samples:

$$d_{i,j} = \frac{1}{N_i(N_i - 1)} \sum_{k,l=1}^{N_i} \left| p_{i,j,k} - p_{i,j,l} \right|, \quad k \neq l, \tag{14}$$

then the mean distance of all conditions is obtained:

$$d_j^W = \frac{1}{C} \sum_{i=1}^{C} d_{i,j}. \tag{15}$$

(2) The mean value of the features is obtained:

$$u_{i,j} = \frac{1}{N_i} \sum_{k=1}^{N_i} p_{i,j,k}, \tag{16}$$

then the average distance of various conditions is gained:

$$d_j^b = \frac{1}{C(C-1)} \sum_{i,m=1}^{C} \left| u_{i,j} - u_{m,j} \right|, \quad i \neq m. \tag{17}$$

(3) The effectiveness factor α_j' is obtained:

$$\alpha_j = \frac{d_j^b}{d_j^W}, \tag{18}$$

$$\alpha_j' = \frac{\alpha_j}{\max(\alpha_j)}, \quad \alpha_j' \in [0, 1]. \tag{19}$$

In the end, the features with larger α_j' are selected to be the salient features.

4. MMC-FCH

Inspired by the basic theory of SVM and flexible convex hull, MMC-FCH method was proposed by Zeng [20, 21]. The main idea of MMC-FCH is replacing the convex hull in SVM with the flexible convex hull, while the optimized hyperplane is obtained by the same approach as SVM.

A convex hull in SVM is considered to be a convex combination of a data set as all the combination parameters amount to one and are nonnegative. For $X = \{x_i\}_{i=1}^N$, the convex hull is defined as follows:

$$\mathrm{CH}(X) = \left\{ \sum_{i=1}^{N} a_i x_i \;\middle|\; \sum_{i=1}^{N} a_i = 1,\ 0 \le a_i \le 1 \right\}. \tag{20}$$

Normally, the tightest convex approximation of the class region of the data is gained by using the convex hull. Nevertheless, for the classes with complicated convex forms, the convex hull is not accurate enough as the class region always extends beyond it. It can be inferred that convex hull should be made looser to fit more complicated situations. Therefore, reference [20] used a new model which is called flexible convex hull instead of the convex hull applied in SVM. The improvement of the flexible convex hull is that it

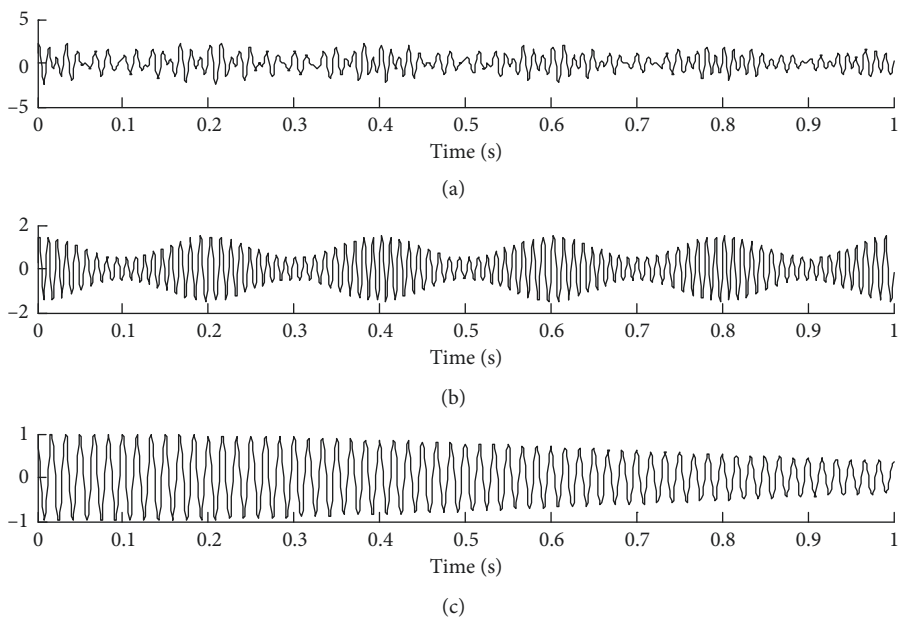

Figure 3: The time-domain waveforms of simulation signal $x_1(n)$ in equation (8) and its components. (a) The mixed signal $x_1(n)$; (b) the AM-FM component; (c) the attenuating component.

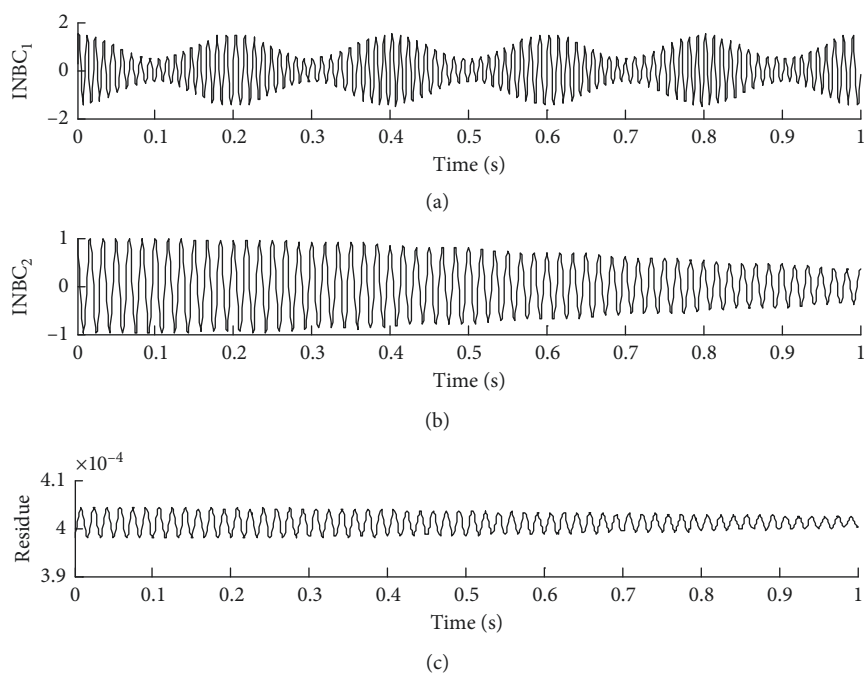

Figure 4: The decomposition results of $x_1(n)$ generated by ASNBD.

uses a flexibility factor μ to construct the bounds of the coefficients. Flexible convex hull is defined as follows:

$$\mathrm{FCH}(X) = \left\{ \sum_{i=1}^{N} a_i x_i \,\middle|\, \sum_{i=1}^{N} a_i = 1,\ \frac{1-\mu}{n} \le a_i \le \frac{1-\mu}{n} + \mu \right\}, \quad \mu \in [1, +\infty). \tag{21}$$

For a prescribed μ, a data point $x_i \in X$ expands along with $\overrightarrow{\overline{x}x_i}$. $\overline{x} = \sum_{i=1}^{N} x_i/n$ is the average of X. Then the expanded $x_i' = \pi(1-\mu)\overline{x} + \mu x_i$ is obtained by calculation to construct the flexible convex hull $X' = \{x_i'\}_{i=1}^{N}$. The bounds of coefficients can be different by applying the flexible convex hull. It can be easily inferred that flexible convex hull becomes convex hull when $\mu = 1$; thus, convex hull is a special situation of the flexible convex hull. If $\mu > 1$, then the flexible

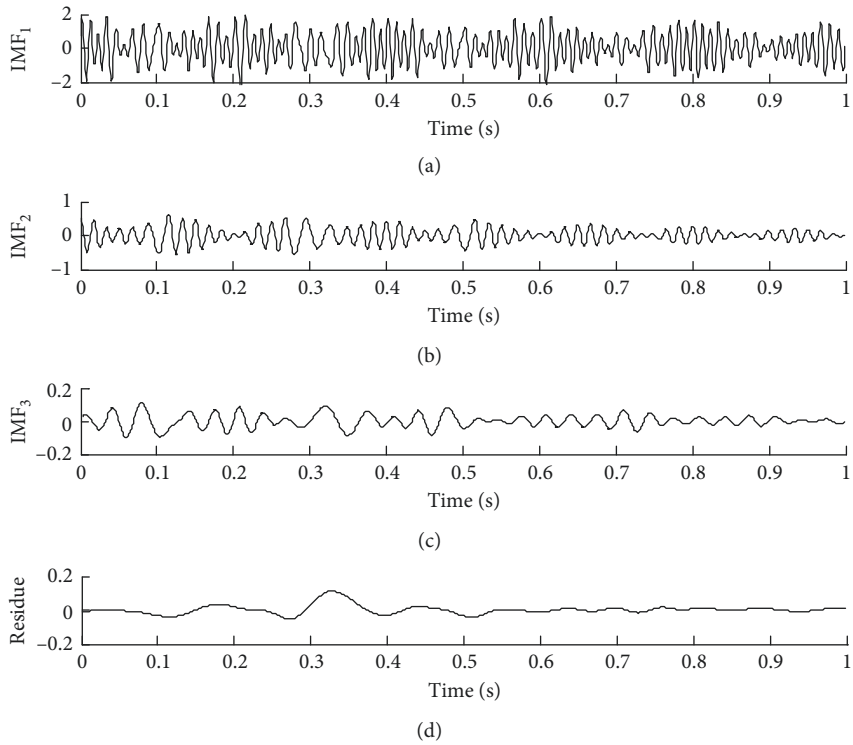

Figure 5: The decomposition results of $x_1(n)$ generated by EMD.

Table 1: Evaluating parameters of the components of $x_1(n)$ generated by ASNBD and EMD.

Method	r_1	r_2	E_1	E_2	IO	T(s)
ASNBD	0.9998	0.9996	3.8497×10^{-4}	7.2631×10^{-4}	0.0021	1.6904
EMD	0.8590	0.6333	0.2621	4.0948	0.0367	0.2018

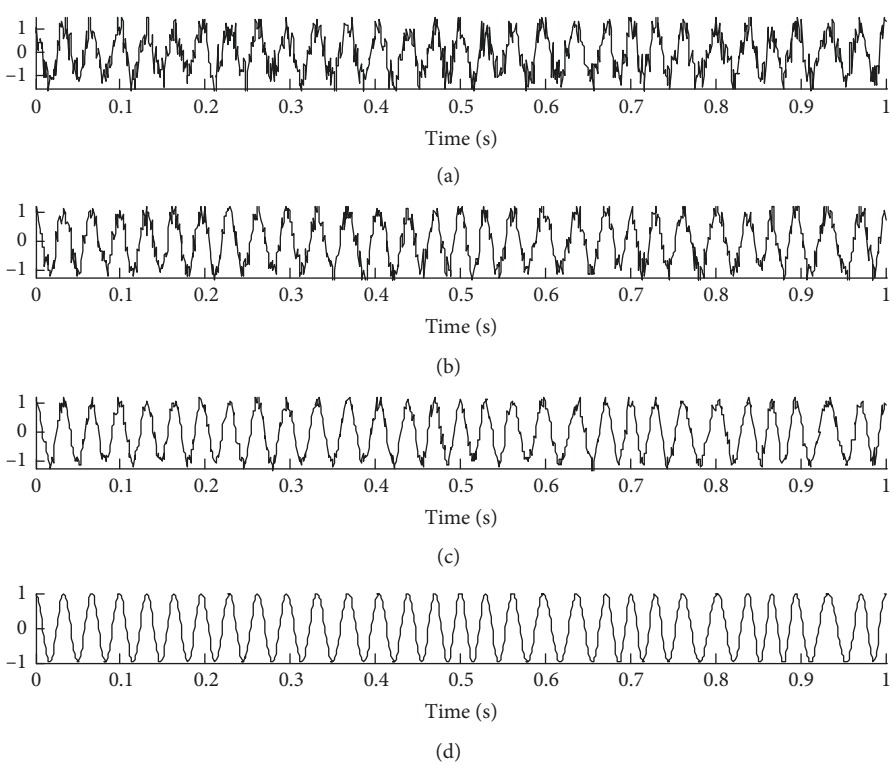

Figure 6: Continued.

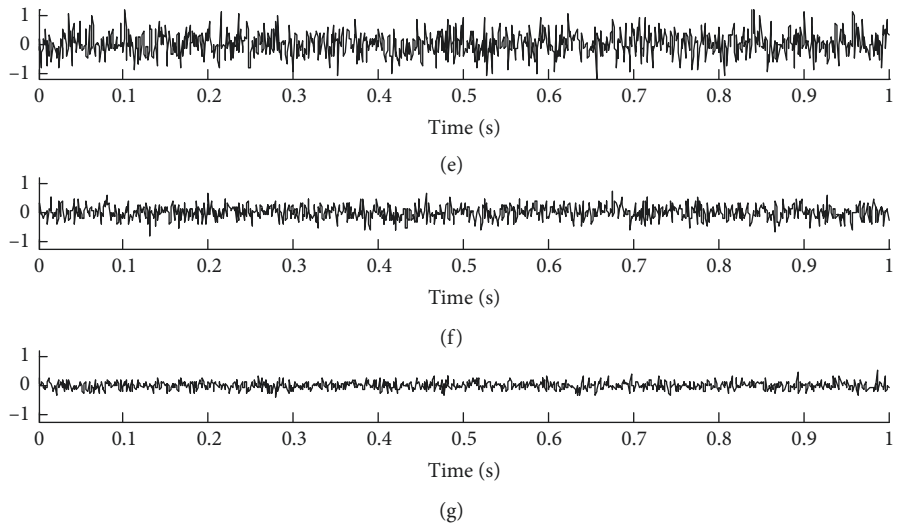

FIGURE 6: The time-domain waveforms of simulation signal $x_2(n)$ in equation (12) and its components. (a), (b), and (c) the mixed signal $x_2(n)$ as SNR = 5, 10, 15, respectively; (d) the AM-FM component of $x_2(n)$; (e), (f), and (g) the noise components $s(n)$ of the signals shown in (a), (b), and (c), respectively.

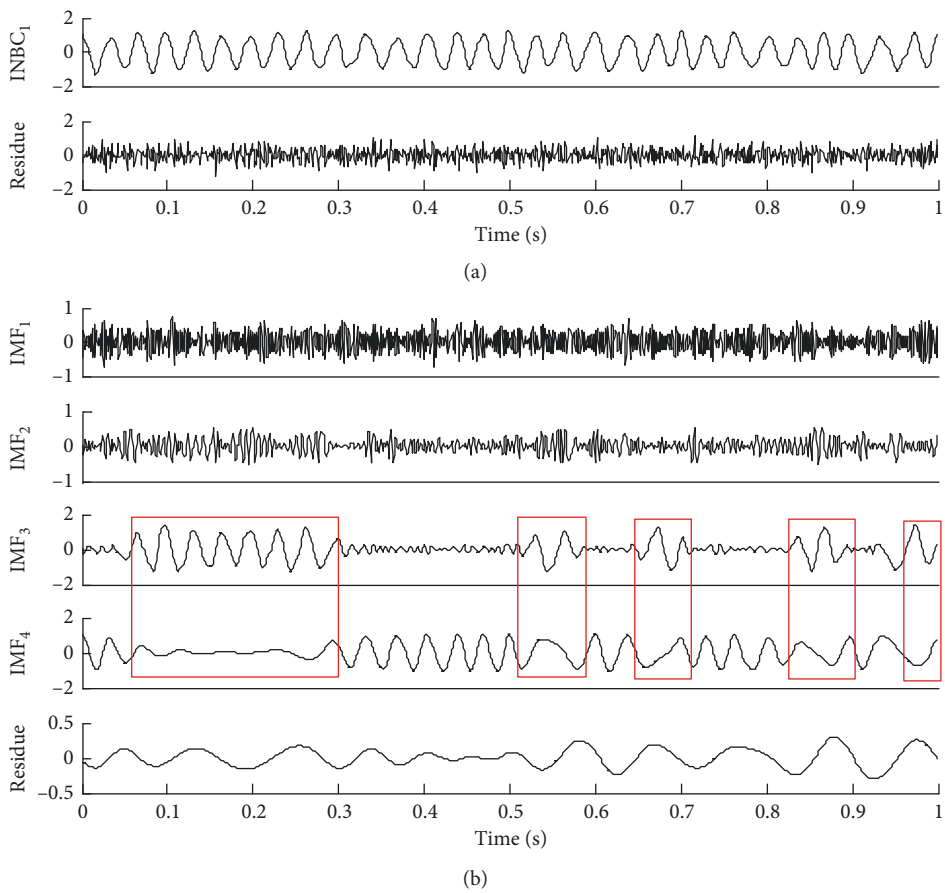

FIGURE 7: The decomposition results generated by ASNBD and EMD of simulation signal $x_2(n)$ shown in Figure 6(a) (SNR = 5). The decomposition results of (a) ASNBD; (b) EMD.

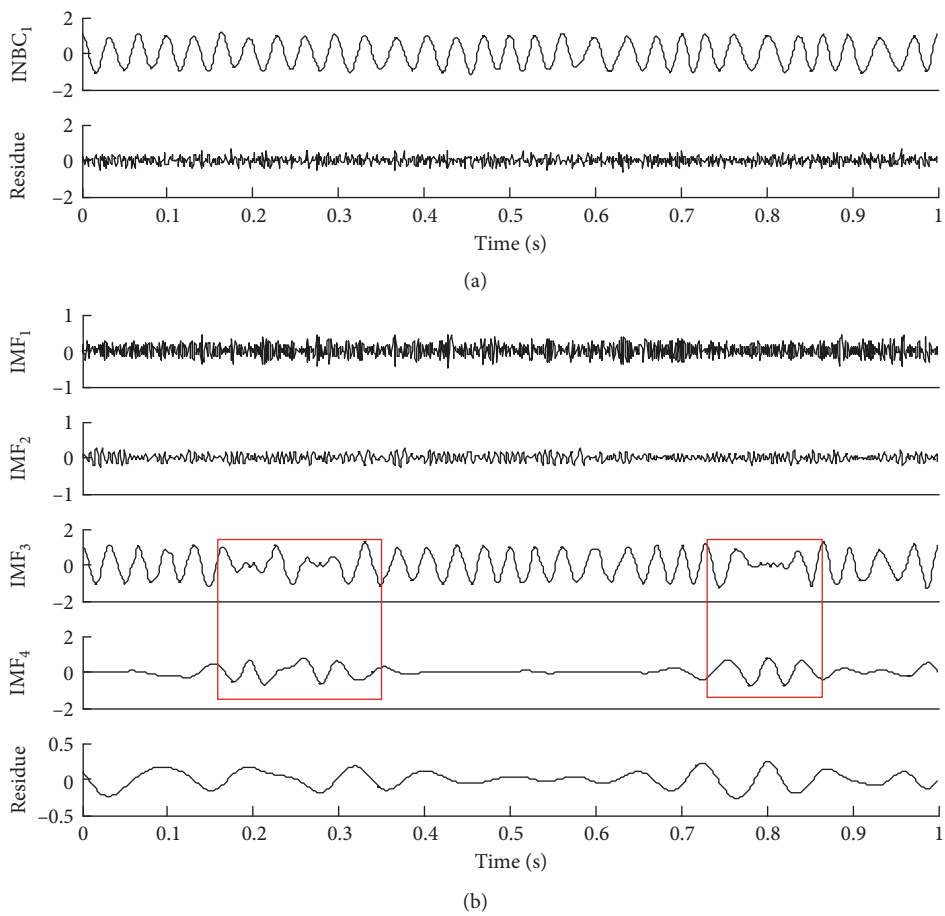

Figure 8: The decomposition results generated by ASNBD and EMD of simulation signal $x_2(n)$ shown in Figure 6(b) (SNR = 10). The decomposition results of (a) ASNBD; (b) EMD.

convex hull becomes looser than the convex hull. If the flexible factor is set appropriately, it is possible that a nice approximation of the class region can be obtained.

The main difference between MMC-FCH and SVM is that MMC-FCH uses flexible convex hull instead of convex hull to get a more satisfactory matching of the class region. The method of obtaining the optimal hyper-plane of the two methods is similar. More details of MMC-FCH can be found in references [20, 21]. Results in reference [20] have already shown that MMC-FCH performed better than SVM when applied to the recognition of roller bearing fault type. Hence, no more comparison is made between MMC-FCH and SVM in this paper as it is unnecessary.

5. The Proposed Method and Experimental Analysis

5.1. The Proposed Method. By applying ASNBD, DET, and MMC-FCH, an approach for mechanical fault diagnosis is proposed. Figure 10 shows the flow chart of the proposed method. The main calculation procedure is as follows:

(1) Decompose the experimental signals by using ASNBD, suppose every data set is decomposed into M INBCs

(2) Calculate the features (shown in Table 3) of the training signals and the INBCs

(3) The normalized effectiveness factors α_j' are calculated; then salient features are selected by applying DET

(4) Classify the fault type by training and testing with MMC-FCH using the salient features

5.2. Experimental Analysis. The experimental data are offered by Case Western Reserve University [27–31]. The experimental system is shown in Figure 11. The type of all the tested bearings is 6205-2RS JEM SKF. Several single-point faults were separately set to the tested roller bearings to generate three fault types including inner race, outer race, and ball fault (the location of outer race faults is 6 o'clock). The fault diameters were set to be 0.021 in., 0.014 in., and 0.007 in., which implied that there were three categories of the degrees of the roller bearing faults: severe, moderate, and slight. The vibration data sets which were collected at the motor housing's drive end are used. The sampling frequency, rotating speed, and the number of the points of each sample were 12 kHz, 1797 rpm, and 4000, respectively. The details about these

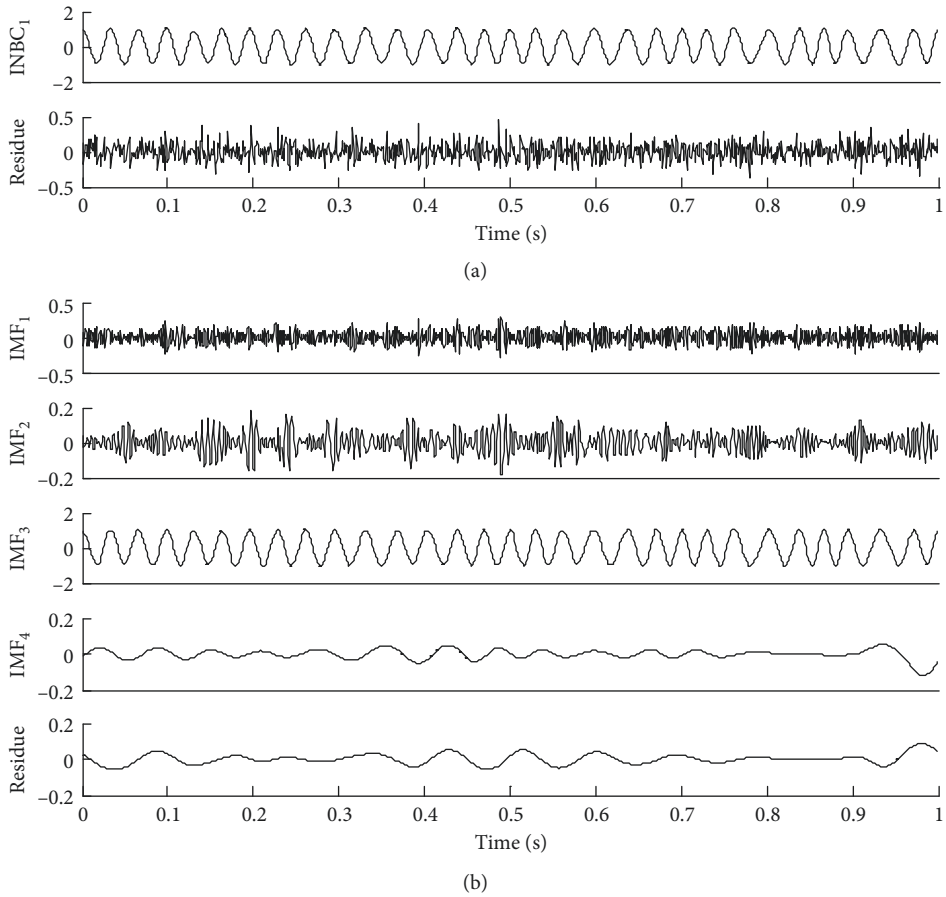

Figure 9: The decomposition results generated by ASNBD and EMD of simulation signal $x_2(n)$ shown in Figure 6(c) (SNR = 15). The decomposition results of (a) ASNBD; (b) EMD.

Table 2: Evaluating parameters of the components of $x_2(n)$ generated by ASNBD and EMD.

Method	SNR	r_1	E_1	IO	T(s)
ASNBD	5	0.9765	0.0468	0.0011	2.6874
	10	0.9930	0.0143	0.0021	1.8205
	15	0.9984	0.0032	0.0054	2.3370
EMD	5	0.6450	1.0284	0.0259	0.3211
	10	0.9082	0.1929	0.0436	0.2103
	15	0.9955	0.0091	0.0073	0.2679

bearing data sets are given in Table 4. Data sets in Table 4 cover ten conditions and each condition contains 30 samples.

5.2.1. Experiment 1. In experiment 1, the ten classes of fault type are considered to be classified by MMC-FCH. Firstly, to compare the performance of EMD and ASNBD on extracting useful features from the original vibration signals, all the 300 data sets are decomposed into eight components by ASNBD and EMD, respectively. The examples of the vibration data samples from each class are shown in Figure 12. The decomposition results of a data sample from class 2 by applying ASNBD and EMD are given in Figures 13 and 14. Then the features from Table 3 of the original signals and the components are calculated. DET is used for choosing salient features, the normalized effectiveness factors of the features which are larger than 0.5 are chosen, and the results are shown in Figures 15 and 16. To assess the proposed method when the number of training data samples varies, 1, 2, 3, 4, 5, 10, 15, 20, and 25 signals of every class were randomly chosen to construct the training samples as well as the rest samples are utilized for testing. The whole test process was repeated for 20 times so that the influence of randomness on the results of classifications can be alleviated. The final classification accuracy in Tables 5 and 6 are the mean values of the 20 results. The flexible factor is set to 1.82 in this experiment.

There are 20 salient features when ASNBD is applied and 15 salient features when EMD is applied, which indicates

Table 3: Statistical parameters.

Frequency domain statistical parameters		Time-domain statistical parameters	
Mean $p_1 = 1/N\sum_{n=1}^{N} x(n)$	Skewness $p_1 = 1/(N-1)\sum_{n=1}^{N}(x(n)-p_1/p_6)^3$	Spectral amplitude mean $p_1 = 1/M\sum_{n=1}^{N} s(k)$	Spectral root 4/2-moment ratio $p_{19} = \sqrt{\sum_{k=1}^{M} f^4(k)s(k)/\sum_{k=1}^{M} f^2(k)s(k)}$
Root mean square $p_2 = \sqrt{1/N\sum_{n=1}^{N} x^2(n)}$	Kurtosis $p_8 = 1/(N-1)\sum_{n=1}^{N}(x(n)-p_1/p_6)^4$	Spectral amplitude standard deviation $p_{14} = \sqrt{1/(M-1)\sum_{k=1}^{M}(s(k)-p_{13})^2}$	Spectral standard deviation frequency $p_{20} = \sqrt{\sum_{k=1}^{M}(f(k)-p_{17})^2\, s(k)/\sum_{k=1}^{M} s(k)}$
Square root amplitude $p_3 = 1/N\sum_{n=1}^{N}\sqrt{\lvert x(n)\rvert}^2$	Crest factor $p_9 = p_5/p_2$	Spectral amplitude skewness $p_{15} = \sqrt{1/(M-1)\sum_{k=1}^{M}((s(k)-p_{13})/p_{14})^3}$	Spectral frequency skewness $p_{21} = \sum_{k=1}^{M}((f(k)-p_{17}/p_{20})^3 s(k))/\sum_{j=1}^{M} s(j)$
Mean amplitude $p_4 = 1/N\sum_{n=1}^{N}\lvert x(n)\rvert$	Clearance factor $p_{10} = p_5/p_3$	Spectral amplitude kurtosis $p_{16} = \sqrt{1/(M-1)\sum_{k=1}^{M}((s(k)-p_{13})/p_{14})^4}$	Spectral frequency kurtosis $p_{21} = \sum_{k=1}^{M}((f(k)-p_{17}/p_{20})^3 s(k))/\sum_{j=1}^{M} s(j)$
Maximum peak $p_5 = 1/2(\max(x(n)) - \min(x(n)))$	Shape factor $p_{11} = p_2/p_4$	Spectral gravity frequency $p_{17} = \sum_{k=1}^{M} f(k)s(k)/\sum_{k=1}^{M} s(k)$	
Standard deviation $p_6 = \sqrt{1/(N-1)\sum_{n=1}^{N}(x(n)-p_1)^2}$	Crest factor $p_{12} = p_5/p_4$	Spectral root mean square frequency $p_{18} = \sqrt{\sum_{k=1}^{M} f^2(k)s(k)/\sum_{k=1}^{M} s(k)}$	

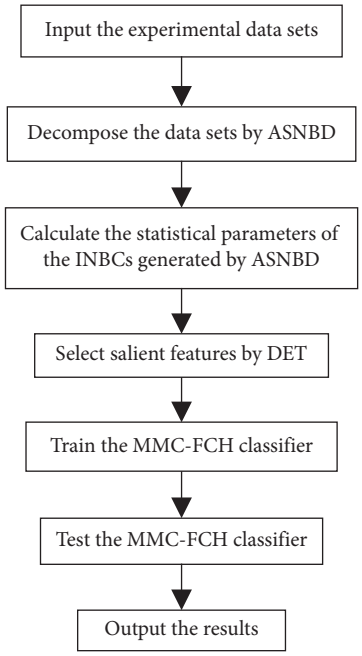

Figure 10: The flow chart of the method proposed in section 5.1.

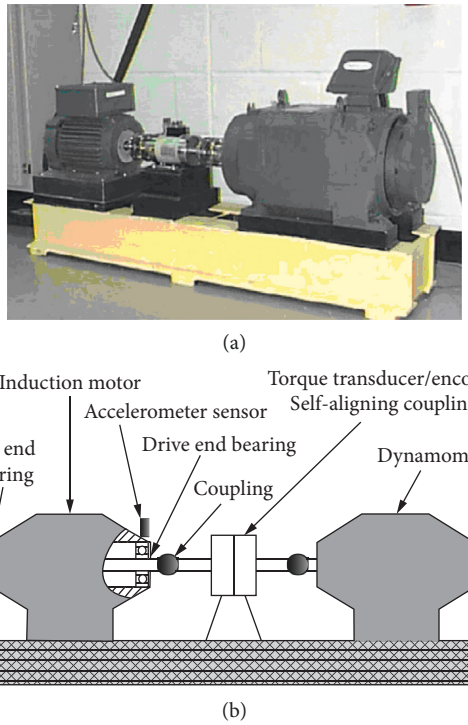

Figure 11: The schematic diagram of roller bearing testbed system.

that ASNBD can extract more effective features than EMD at least in this experiment. Results in Table 5 show that ASNBD and EMD both can generate satisfying classification accuracy. The accuracy is above 90% even when there is only one training sample. However, the classification accuracies of ASNBD are always higher than EMD in this experiment. Thus, ASNBD is more effective in the analysis of experiment 1 when the fault locations and fault severity varies.

5.2.2. Experiment 2. The severity of the faults is ignored and only the locations of the faults are identified in this

Table 4: Descriptions of the experimental data sets.

Fault class	Fault severity	Defect size (in.)	Number of data sets	Class label
Normal	No fault	0	30	1
Ball fault	Slight	0.007	30	2
Ball fault	Moderate	0.014	30	3
Ball fault	Severe	0.021	30	4
Inner race fault	Slight	0.007	30	5
Inner race fault	Moderate	0.014	30	6
Inner race fault	Severe	0.021	30	7
Outer race fault	Slight	0.007	30	8
Outer race fault	Moderate	0.014	30	9
Outer race fault	Severe	0.021	30	10

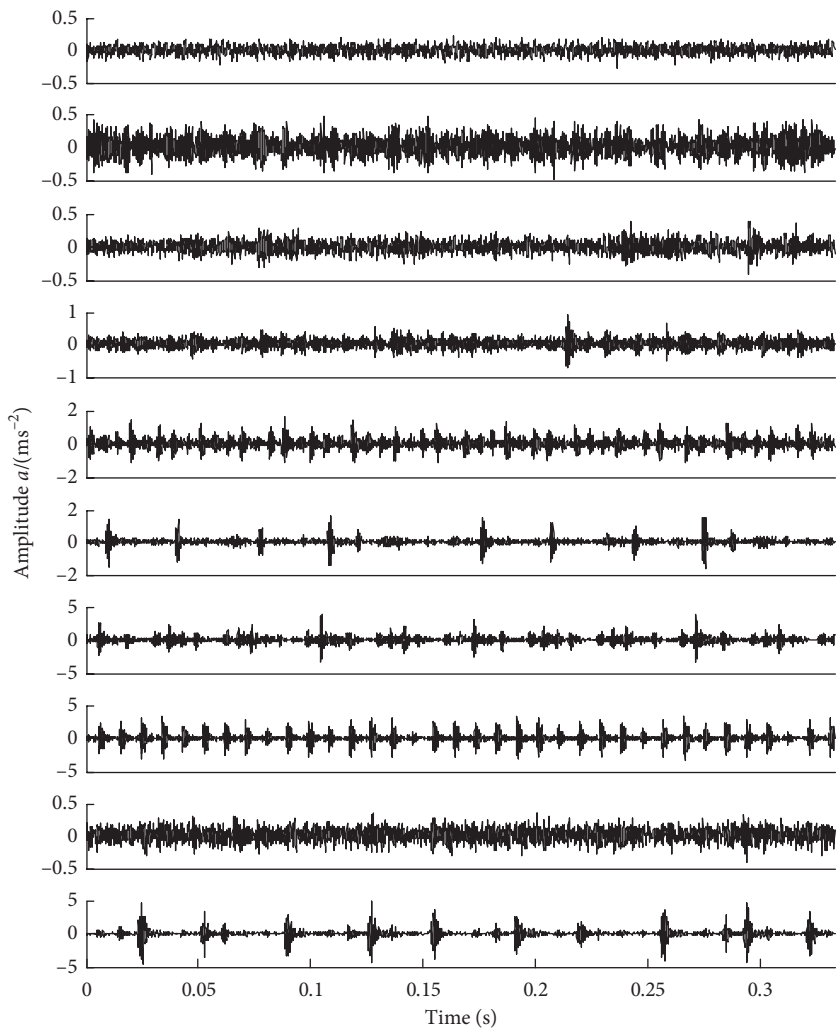

Figure 12: Vibration signals of each class. From top to bottom, the class labels of the vibration signals are 1, 2, 3, 4, 5, 6, 7, 8, 9, and 10, respectively.

experiment. Thus, only 4 faults consisting of ball fault, regular condition, inner fault, and outer fault are considered. As there are 30 samples from the regular condition and 90 samples from every other condition, 30 samples are randomly chosen from the 90 samples of inner fault or outer fault. The sample partitions of this experiment are just like those of experiment 1. As all the data sets are decomposed into eight components by ASNBD and EMD, there are still 198 statistical parameters for testing the effectiveness of both ASNBD and EMD. In this experiment, the normalized effectiveness factors of the features which are bigger than 0.8 are chosen. Salient features of the components obtained by

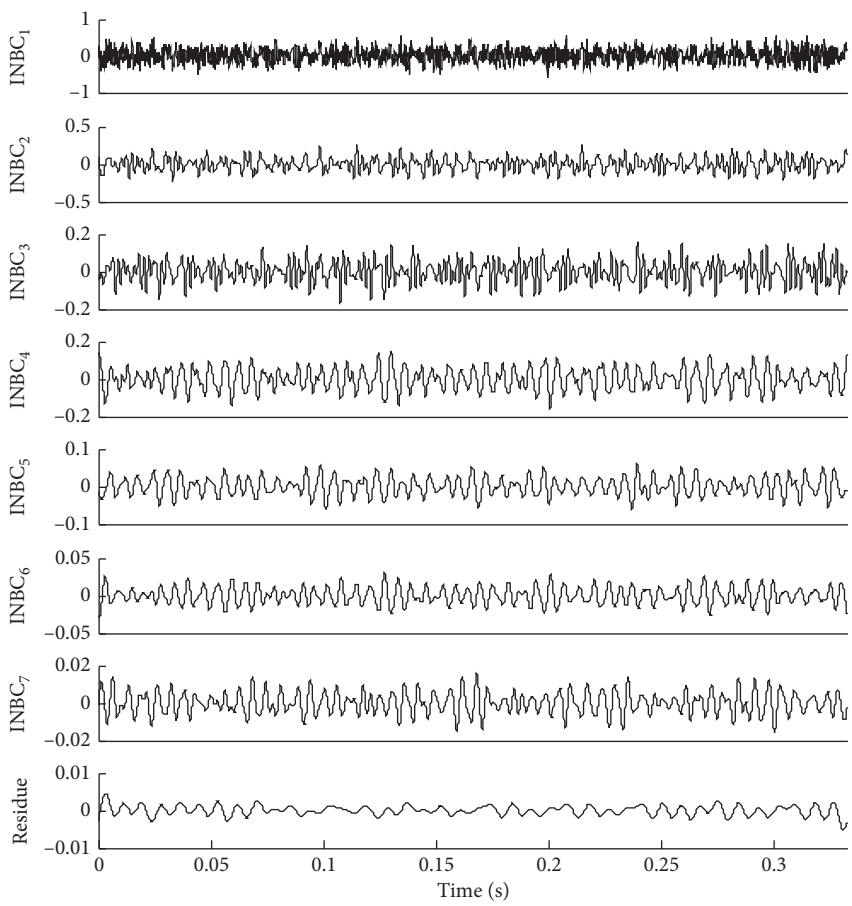

Figure 13: The decomposing results generated by ASNBD of a vibration signal from class 2.

EMD and ASNBD in experiment 2 are shown in Figures 17 and 18. The flexible factor is set to 2.59 in this experiment.

There are 15 salient features when ASNBD is applied and 12 salient features when EMD is applied; thus, ASNBD still extracts more effective features than EMD in experiment 2. Results in Table 6 show that the accuracies are above 90% when the training samples are more than 5, while the classification accuracy drops rapidly when the number of the samples is very few (less than or equal to 5). This is because that the classification has become more difficult when the severity of the faults are ignored, since the samples with the same fault locations still have intrinsic differences when the fault severity varies. Even so, ASNBD still outperforms EMD.

Experiment 1 is conducted for analyzing the effectiveness of the proposed method when applying to recognize rolling bearing with different fault types, and experiment 2 is conducted for recognizing the fault locations. Experiments 1 and 2 show that ASNBD and EMD both show a satisfying performance on identifying different fault types of roller bearings when combined with MMC-FCH. Moreover, ASNBD is superior to EMD, either the samples can be easily classified (experiment 1) or the recognition task is relatively difficult (experiment 2). However, the mean time of the identification process of every data set shown in Tables 5 and 6 shows that ASNBD still costs more calculation than EMD when combined with MMC-FCH.

6. Conclusions

ASNBD is proposed by applying the idea of EMD and MP for nonstationary signal analysis. The theoretical analysis indicates that the proposed method excels MP in both the physical meaning and the adaptivity. And problems like end effect and mode mixing of EMD are reduced because the application of interpolation function is not required. The simulation analysis results show that ASNBD excels EMD in the accuracy of the decomposition results, the orthogonality and the antinoise performance. Furthermore, ASNBD is applied to classify the roller bearing fault. The vibration signals of roller bearings with fault are decomposed by ASNBD at first. Then DET is utilized to choose salient features of the generated components. To fulfill the fault diagnosis, the new classification method MMC-FCH is introduced to identify the fault types of roller bearings automatically. The experimental analysis indicates that ASNBD not only shows a satisfying performance on identifying different fault types of roller bearings when combined with MMC-FCH, but also is superior to EMD on extracting accurate fault features.

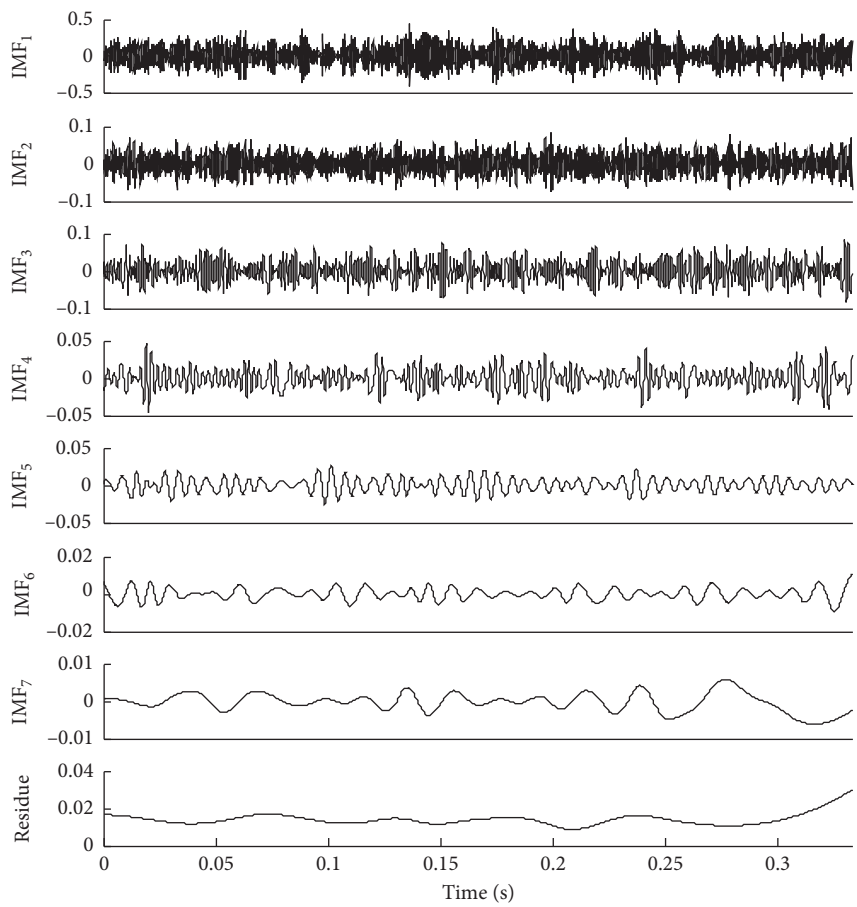

Figure 14: The decomposing results generated by EMD of a vibration signal from class 2.

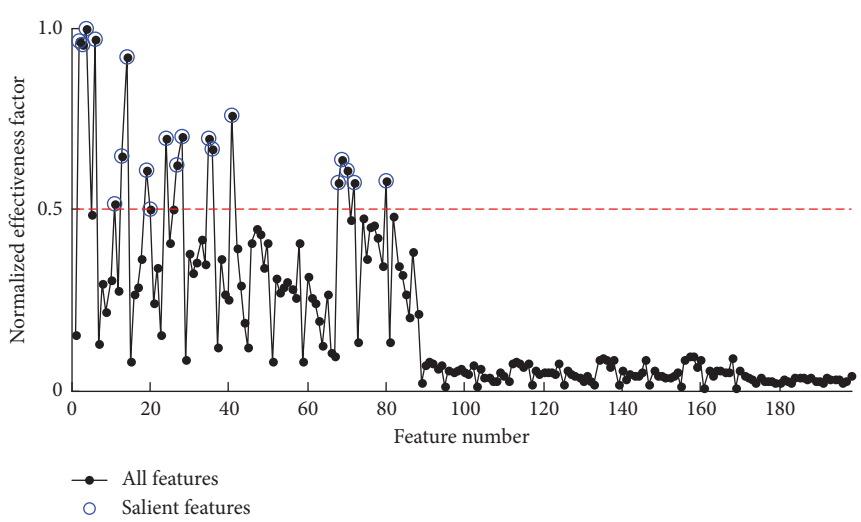

Figure 15: Salient features when ASNBD is applied in experiment 1.

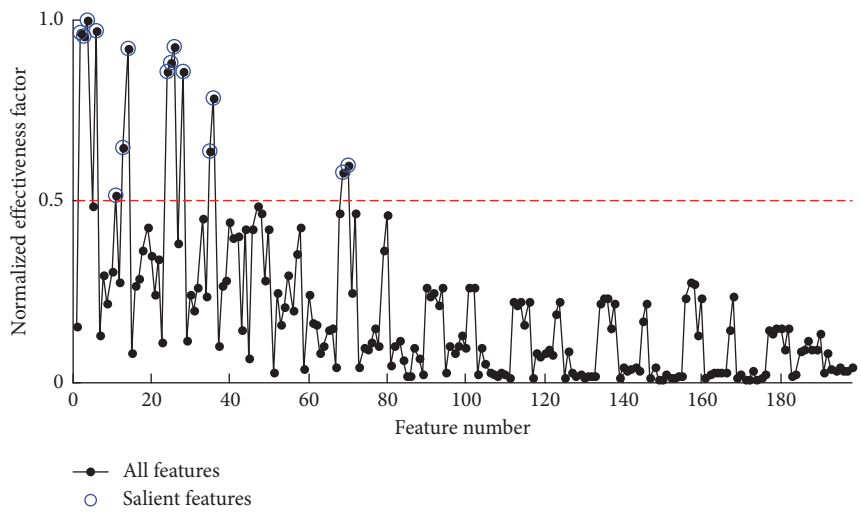

Figure 16: Salient features when EMD is applied in experiment 1.

Table 5: Classification accuracy of MMC-CH ($n = 1, 2, ..., N$) in experiment 1.

Decomposition method	Classification accuracy (%) when the number of training samples varies									Mean time (s)
	1	2	3	4	5	10	15	20	25	
ASNBD	91.59	95.35	96.73	98.06	98.14	99.32	99.40	99.65	99.70	12.53s
EMD	90.60	94.66	95.93	97.13	97.58	99.17	99.03	99.45	99.50	2.31s

Table 6: Classification accuracy of MMC-CH (P_1) in experiment 2.

Decomposition method	Classification accuracy (%) when the number of training samples varies									Mean time (s)
	1	2	3	4	5	10	15	20	25	
ASNBD	71.59	76.91	79.08	87.17	88.82	93.98	94.91	95.07	95.25	15.26
EMD	68.39	74.66	78.98	84.44	86.90	91.33	92.34	92.14	93.95	1.87

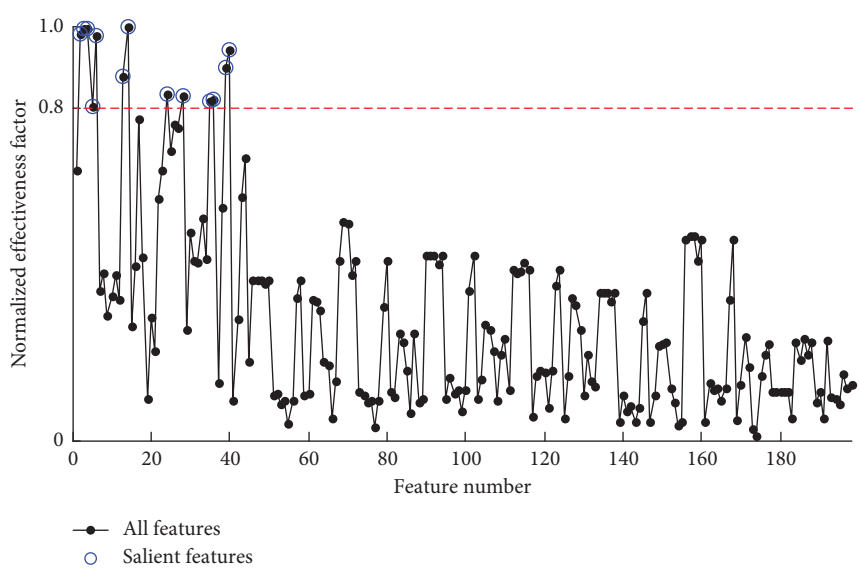

Figure 17: Salient features when ASNBD is applied in experiment 2.

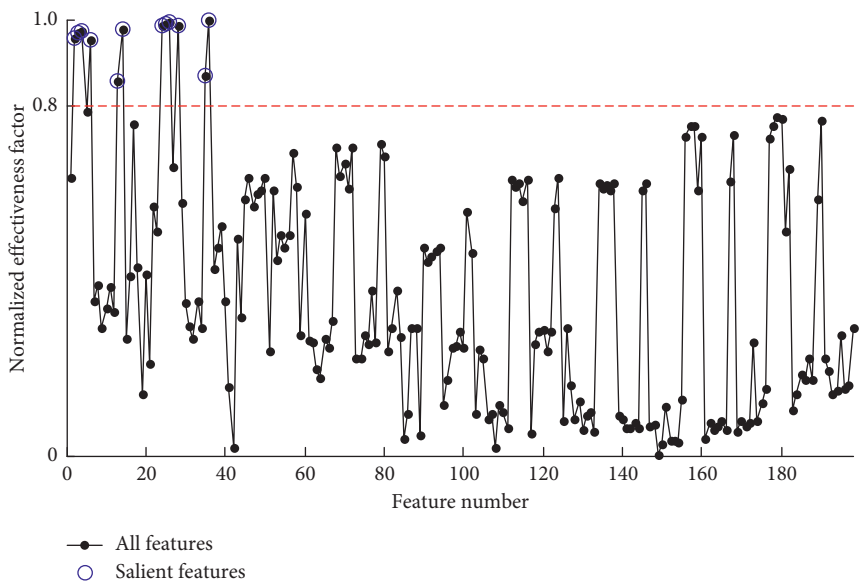

Figure 18: Salient features when EMD is applied in experiment 2.

Data Availability

Previously reported .mat data were used to support this study and are available at DOI: 10.1016/j.ymssp.2015.04.021. These prior studies (and data sets) are cited at relevant places within the text as references [23].

Conflicts of Interest

The authors declare that they have no conflicts of interest.

Acknowledgments

This work was supported by the National Key Research and Development Program of China (2018YFF0212902), National Natural Science Foundation of China (51805161, 51475159, and 51575178), Hunan Provincial Key Research and Development Program (2018GK2044), and Hunan Provincial Natural Science Foundation of China (2018JJ3187, 2017JJ1015, 2017JJ2086, and 2018JJ4084).

References

[1] S. G. Mallat and Z. Zhifeng Zhang, "Matching pursuits with time-frequency dictionaries," *IEEE Transactions on Signal Processing*, vol. 41, no. 12, pp. 3397–3415, 1993.

[2] H. Yang, J. Mathew, and L. Ma, "Fault diagnosis of rolling element bearings using basis pursuit," *Mechanical Systems and Signal Processing*, vol. 19, no. 2, pp. 341–356, 2005.

[3] X. Liu, L. Bo, X. He, and M. Veidt, "Application of correlation matching for automatic bearing fault diagnosis," *Journal of Sound and Vibration*, vol. 331, no. 26, pp. 5838–5852, 2012.

[4] N. E. Huang, Z. Shen, S. R. Long et al., "The empirical mode decomposition and the Hilbert spectrum for nonlinear and non-stationary time series analysis," *Proceedings of the Royal Society of London. Series A: Mathematical, Physical and Engineering Sciences*, vol. 454, no. 1971, pp. 903–995, 1998.

[5] J. Cheng, D. Yu, J. Tang, and Y. Yang, "Application of frequency family separation method based upon EMD and local Hilbert energy spectrum method to gear fault diagnosis," *Mechanism and Machine Theory*, vol. 43, no. 6, pp. 712–723, 2008.

[6] J. Cheng, D. Yu, J. Tang, and Y. Yang, "Local rub-impact fault diagnosis of the rotor systems based on EMD," *Mechanism and Machine Theory*, vol. 44, no. 4, pp. 784–791, 2009.

[7] G. Gai, "The processing of rotor startup signals based on empirical mode decomposition," *Mechanical Systems and Signal Processing*, vol. 20, no. 1, pp. 225–235, 2006.

[8] J. C. Nunes, S. Guyot, and E. Deléchelle, "Texture analysis based on local analysis of the bidimensional empirical mode decomposition," *Machine Vision and Applications*, vol. 16, no. 3, pp. 177–188, 2005.

[9] M. Dätig and T. Schlurmann, "Performance and limitations of the Hilbert-Huang transformation (HHT) with an application to irregular water waves," *Ocean Engineering*, vol. 31, no. 14-15, pp. 1783–1834, 2004.

[10] W. G. Huang, G. Gao, N. Li et al., "Time-frequency squeezing and generalized demodulation combined for variable speed bearing fault diagnosis," *IEEE Transactions on Instrumentation and Measurement*, vol. 68, no. 8, pp. 2819–2829, 2019.

[11] J. Cheng, D. Yu, and Y. Yang, "Application of support vector regression machines to the processing of end effects of Hilbert-Huang transform," *Mechanical Systems and Signal Processing*, vol. 21, no. 3, pp. 1197–1211, 2007.

[12] L. Cui, X. Wang, H. Wang, and N. Wu, "Improved fault size estimation method for rolling element bearings based on concatenation dictionary," *IEEE Access*, vol. 7, pp. 22710–22718, 2019.

[13] J.-L. Starck, M. Elad, and D. Donoho, "Redundant multiscale transforms and their application for morphological component separation," *Advances in Imaging and Electron Physics*, vol. 132, pp. 287–348, 2004.

[14] A. Lobo and P. Loizou, "Voiced/unvoiced speech discrimination in noise using Gabor atomic decomposition," in *Proceeding of the IEEE International Conference on Acoustics Speech, and Signal Processing*, Hong Kong, China, 2003.

[15] J.-L. Starck, M. Elad, and D. L. Donoho, "Image decomposition via the combination of sparse representations

and a variational approach," *IEEE Transactions on Image Processing*, vol. 14, no. 10, pp. 1570–1582, 2005.

[16] N. Li, W. G. Huang, W. J. Guo et al., "Multiple Enhanced Sparse Decomposition for gearbox compound fault diagnosis," *IEEE Transactions on Instrumentation and Measurement*, pp. 1–12, 2019.

[17] L. Cui, X. Wang, Y. Xu, H. Jiang, and J. Zhou, "A novel Switching Unscented Kalman Filter method for remaining useful life prediction of rolling bearing," *Measurement*, vol. 135, pp. 678–684, 2019.

[18] J. Cheng, Y. Peng, Y. Yang, and Z. Wu, "Adaptive sparsest narrow-band decomposition method and its applications to rolling element bearing fault diagnosis," *Mechanical Systems and Signal Processing*, vol. 85, pp. 947–962, 2017.

[19] S. L. Peng and W. L. Hwang, "Adaptive signal decomposition based on local narrow band signals," *IEEE Transactions on Signal Processing*, vol. 56, no. 7, pp. 2669–2676, 2008.

[20] M. Zeng, Y. Yang, J. Zheng, and J. Cheng, "Maximum margin classification based on flexible convex hulls for fault diagnosis of roller bearings," *Mechanical Systems and Signal Processing*, vol. 66-67, pp. 533–545, 2016.

[21] M. Zeng, Y. Yang, J. Zheng, and J. Cheng, "Maximum margin classification based on flexible convex hulls," *Neurocomputing*, vol. 149, pp. 957–965, 2015.

[22] B. S. Yang, T. Han, and J. L. An, "ART-KOHONEN neural network for fault diagnosis of rotating machinery," *Mechanical Systems and Signal Processing*, vol. 18, no. 3, pp. 645–657, 2004.

[23] B.-S. Yang, T. Han, and W.-W. Hwang, "Fault diagnosis of rotating machinery based on multi-class support vector machines," *Journal of Mechanical Science and Technology*, vol. 19, no. 3, pp. 846–859, 2005.

[24] D. Ho and R. B. Randall, "Optimisation of bearing diagnostic techniques using simulated and actual bearing fault signals," *Mechanical Systems and Signal Processing*, vol. 14, no. 5, pp. 763–788, 2000.

[25] J. Antoni, "Cyclic spectral analysis of rolling-element bearing signals: facts and fictions," *Journal of Sound and Vibration*, vol. 304, no. 3–5, pp. 497–529, 2007.

[26] D.-C. Lin, Z.-L. Guo, F.-P. An, and F.-L. Zeng, "Elimination of end effects in empirical mode decomposition by mirror image coupled with support vector regression," *Mechanical Systems and Signal Processing*, vol. 31, pp. 13–28, 2012.

[27] http://csegroups.case.edu/bearingdatacenter/pages/download-data-file.

[28] W. A. Smith and R. B. Randall, "Rolling element bearing diagnostics using the Case Western Reserve University data: a benchmark study," *Mechanical Systems and Signal Processing*, vol. 64-65, pp. 100–131, 2015.

[29] K. He and X. Li, "A quantitative estimation technique for welding quality using local mean decomposition and support vector machine," *Journal of Intelligent Manufacturing*, vol. 27, no. 3, pp. 525–533, 2016.

[30] K. He, Q. Li, and J. Chen, "An arc stability evaluation approach for SW AC SAW based on Lyapunov exponent of welding current," *Measurement*, vol. 46, no. 1, pp. 272–278, 2013.

[31] K. He, Z. Zhang, S. Xiao, and X. Li, "Feature extraction of AC square wave SAW arc characteristics using improved Hilbert-Huang transformation and energy entropy," *Measurement*, vol. 46, no. 4, pp. 1385–1392, 2013.